Hindawi Publishing Corporation
Journal of Biomedicine and Biotechnology
Volume 2011, Article ID 675701, 8 pages
doi:10.1155/2011/675701

Research Article

Investigation of a Potential Scintigraphic Tracer for Imaging Apoptosis: Radioiodinated Annexin V-Kunitz Protease Inhibitor Fusion Protein

Mei-Hsiu Liao,[1,2] Tong-Rong Jan,[3] Chao-Chih Chiang,[2] Kuo-Chen Yen,[2] Tse-Zung Liao,[2] Ming-Wei Chen,[2] Chin-Wen Chi,[1,4] Tze-Chein Wun,[5] Tzu-Chen Yen,[6] and Shiaw-Pyng Wey[6,7]

[1] *Institute of Pharmacology, School of Medicine, National Yang-Ming University, Taipei 112, Taiwan*
[2] *Division of Isotope Application, Institute of Nuclear Energy Research, Taoyuan 325, Taiwan*
[3] *Department of Veterinary Medicine, National Taiwan University, Taipei 106, Taiwan*
[4] *Department of Medical Research and Education, Taipei Veterans General Hospital, Taipei 112, Taiwan*
[5] *EVAS Therapeutics LLC, 613 Huntley Heights Drive, Ballwin, MO 63021, USA*
[6] *Department of Nuclear Medicine and Molecular Imaging Center, Chang Gung Memorial Hospital and Chang Gung University College of Medicine, 259 Wen-Hwa First Road, Kwei-Shan, Taoyuan 333, Taiwan*
[7] *Department of Medical Imaging and Radiological Sciences, Chang Gung University, Taoyuan 333, Taiwan*

Correspondence should be addressed to Tze-Chein Wun, tcwun@hotmail.com and Shiaw-Pyng Wey, spwey@mail.cgu.edu.tw

Received 29 November 2010; Accepted 15 February 2011

Academic Editor: David J. Yang

Radiolabeled annexin V (ANV) has been widely used for imaging cell apoptosis. Recently, a novel ANV-Kunitz-type protease inhibitor fusion protein, ANV-6L15, was found to be a promising probe for improved apoptosis detection based on its higher affinity to phosphatidylserine (PS) compared to native ANV. The present paper investigates the feasibility of apoptosis detection using radioiodinated ANV-6L15. Native ANV and ANV-6L15 were labeled with iodine-123 and iodine-125 using Iodogen method. The binding between the radioiodinated proteins and erythrocyte ghosts or chemical-induced apoptotic cells was examined. ANV-6L15 can be radioiodinated with high yield (40%−60%) and excellent radiochemical purity (>95%). ^{123}I-ANV-6L15 exhibited a higher binding ratio to erythrocyte ghosts and apoptotic cells compared to ^{123}I-ANV. The biodistribution of ^{123}I-ANV-6L15 in mice was also characterized. ^{123}I-ANV-6L15 was rapidly cleared from the blood. High uptake in the liver and the kidneys may limit the evaluation of apoptosis in abdominal regions. Our data suggest that radiolabled ANV-6L15 may be a better scintigraphic tracer than native ANV for apoptosis detection.

1. Introduction

Apoptosis (programmed cell death) plays an important role in the maintenance of physiological homeostasis as well as in the pathogenesis of a number of disorders including cerebral and myocardial ischemia, autoimmune diseases, and neurodegeneration [1–3]. Apoptosis also plays a crucial role in tumor response to radiation, chemotherapy, and photodynamic therapy (PDT) [4]. The extent and time frame of cancer cell apoptosis induced by anticancer treatments provide crucial clinical information on both the disease status and the therapeutic efficacy.

The plasma membrane phospholipids of mammalian cells are normally asymmetrically distributed, in which the phosphatidylserine (PS) and phosphatidylethanolamine (PE) are segregated to the internal leaflet whereas the phosphatidylcholine (PC) and sphingomyelin (SM) reside on the outer leaflet [5, 6]. Once apoptosis has been initiated, the caspase-mediated signaling cascade of cells is activated. One of the earliest events occurred in apoptotic cells is the externalization of PS to the outer leaflet of the plasma membrane.

Annexin V (ANV), an endogenous human protein with a molecular weight of 35.8 kDa, binds to membrane-bound

PS in a Ca^{2+}-dependent manner with a high affinity (K_d = 0.5–7 nM). Since externalization of PS occurs in the early stage of apoptosis, fluorescein- and radionuclide-labeled ANV have been used for detection of apoptosis *in vitro* and under development for *in vivo* imaging as well [3, 7]. However, the physiological concentration of Ca^{2+} is lower than that required for optimal binding of native ANV to PS [8], rendering a suboptimal binding condition for apoptosis detection *in vivo*. In addition, excessive uptake by the liver and the kidney further limits the application of native ANV for *in vivo* apoptosis imaging [9]. In light of these drawbacks of native ANV concerning the *in vivo* detection of apoptosis, the development of derivatives of ANV with an improved binding profile to PS and pharmacokinetic properties has been under intensive investigation recently.

ANV possesses anticoagulant and antithrombotic activity by forming 2-dimensional arrays on anionic membrane surfaces, and thus making the anionic phospholipids unavailable for assembly of coagulation enzyme complexes [10]. In attempts to developing potent thrombogenesis inhibitors, a series of recombinant anticoagulant fusion proteins, consisting of an ANV moiety and a Kunitz protease inhibitor (KPI) domain that binds to various coagulation factors with high affinity and specificity, were reported recently [11]. One of these constructs, ANV-6L15, was found to possess a higher binding affinity to PS compared to native ANV at physiological Ca^{2+} concentrations; the apparent dissociation constant for ANV-6L15 binding to erythrocyte ghosts was approximately 4-fold lower than that of ANV at 1.2–2.5 mM Ca^{2+} [12]. The previous study reveals that ANV-6L15 may provide improved detection of PS exposed on the membrane surfaces of pathological cells *in vitro* and *in vivo*. The present study investigates the use of radioiodinated ANV-6L15 as an imaging agent for apoptosis detection.

2. Materials and Methods

2.1. Materials and Reagents. ^{123}I-NH_4I was produced by a compact cyclotron (Ebco TR30/15, Vancouver, Canada) at the Institute of Nuclear Energy Research (INER, Longtan, Taoyuan, Taiwan). ^{125}I-NaI was supplied by IZOTOP Institute of Isotopes (Budapest, Hungary). Iodogen (1,3,4,6-tetrachloro-3,6-diphenylglycoluril) precoated iodination tubes were purchased from Pierce Biotechnology (Rockford, IL, USA). ANV-6L15 was produced by expression in *Escherichia coli* as described previously [9]. ANV and FITC-ANV apoptosis detection kit were obtained from Becton Dickinson (Franklin Lakes, NJ, USA). Nanosep 10 K Centrifugal Devices were purchased from Pall Life Science (Ann Arbor, MI, USA). Stabilized 5C Cell Control was a generous gift from Beckman Coulter (Fullerton, CA, USA). Camptothecin (CPT) was purchased from Sigma (Cambridge, MA, USA). Acute lymphoblastic cell line of human Jurkat T-cell was obtained from Bioresource Collection and Research Center (Hsinchu, Taiwan). Cell culture materials were obtained from Gibco BRL (Grand Island, NY, USA). All other chemicals were purchased from Merck (Darmstadt, Germany).

2.2. Radioiodination of ANV and ANV-6L15. The Iodogen method [13, 14] was adopted for radiolabeling of ANV and ANV-6L15 with ^{123}I or ^{125}I. Briefly, ten μg of ANV and ANV-6L15 were dissolved in 15 μL of 0.1 M KH_2PO_4 (pH 8) solution and reacted with radioiodide (370 MBq ^{123}I-NH_4I or 185 MBq ^{125}I-NaI) in a tube precoated with 50 μg of Iodogen. After gentle agitation of the tube at room temperature for 10 min, the reaction mixture and the rinse of the tube (with 400 μL 0.01 M KH_2PO_4 solution, pH 7.4) were loaded on a Nanosep 10 K Centrifugal Device prewashed with 400 μL 0.01 M KH_2PO_4 solution (pH 7.4). After centrifugation of the Nanosep tube at 15,000×g for 5 min and washing twice with 400 μL 0.01 M KH_2PO_4 (pH 7.4) solution, the radioiodinated protein on the membrane of Nanosep tube was harvested.

2.3. Radiochemical Analysis by High-Pressure Liquid Chromatography. The radiochemical purities of radioiodinated ANV and ANV-6L15 were determined on an analytical HPLC system (Waters 600E, Milford, MA, USA) equipped with a size-exclusion column (Waters Ultrahydrogel 250 column, 7.8 × 300 mm, 6 μm) and a Waters Ultrahydrogel guard column (6.0 mm × 40 mm, 6 μm). After loading 10 μL of diluted radiolabeled protein, the column was eluted with 0.01 M KH_2PO_4 solution (pH 7.4) at a flow rate of 0.8 mL/min. The radioactivity of the eluate was monitored online by a flow detector (FC-1000, Bioscan, Washington, DC, USA).

2.4. Erythrocyte Ghost Binding Assay. Stabilized erythrocyte ghosts were prepared by hypotonic treatment of 5C Cell Control (Beckman Coulter) to expose more PS sites. The cell control erythrocytes were incubated alternatively with water and 10 mM HEPES buffer (containing 137 mM NaCl, 4 mM KCl, 0.5 mM $MgCl_2$, 0.5 mM NaH_2PO_4, 0.1% D-glucose, and 0.1% BSA; pH 7.4) twice at 37°C for 45 min. Following centrifugation at 16,000×g for 5 min, the pellet of stabilized erythrocytes was resuspended in 10 mM HEPES buffer. For the binding studies, erythrocyte ghosts (1.1×10^9 cells/mL) were incubated with ^{125}I-ANV and ^{125}I-ANV-6L15, respectively, in binding buffers (10 mM HEPES buffer, pH 7.4, with 1.2–10 mM calcium chloride solution) at room temperature for 30 min. Bound and free radioiodinated proteins were then separated by centrifugation at 16,000×g for 10 min. The radioactivities in the pellet and the supernatants were measured using an automatic gamma counter (Wizard 1470, PerkinElmer Wallac, Turku, Finland), and the percentage of radioactivity bound to erythrocyte ghosts was calculated. Binding of ^{125}I-NaI to erythrocyte ghosts served as a negative control.

2.5. Apoptotic Cell Binding Assay. Apoptotic Jurkat T-cells were prepared by treatment with an anticancer drug camptothecin (CPT; 8 μM) for 24 hours [15, 16]. In brief, cell culture flasks with RPMI 1640 medium (5 mL containing 10^7 cells) mixed with CPT-DMSO solution (5 μL; 8 mM) and DMSO (5 μL) served as CPT-treated and vehicle-treated groups, respectively. Apoptosis of Jurkat T-cells was

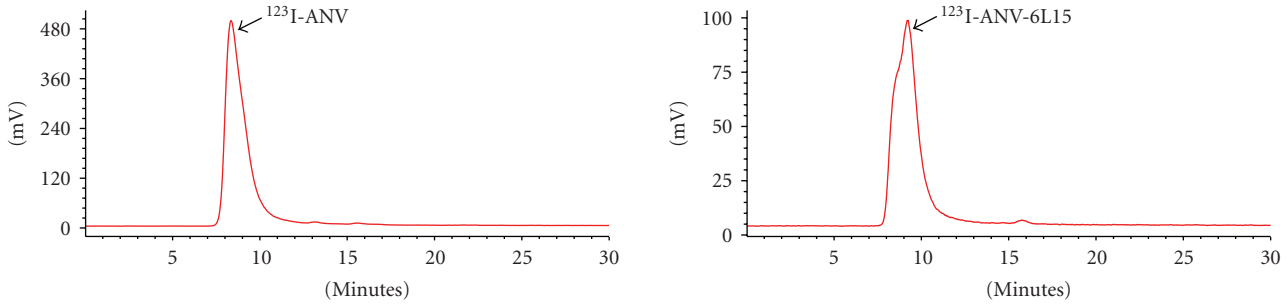

Figure 1: Representative HPLC radiochromatograms of (a) ^{123}I-ANV and (b) ^{123}I-ANV-6L15. HPLC analysis was performed on a Waters Ultrahydrogel 250 column, (7.8 × 300 mm, 6 μm) guarded with a Waters Ultrahydrogel guard column (6.0 mm × 40 mm, 6 μm), with mobile phase of isocratic 0.01 M KH_2PO_4 solution (pH 7.4) at a flow rate of 0.8 mL/min.

confirmed by flow cytometry using FITC-ANV and propidium iodide (PI) staining. Apoptotic cells were identified as ANV^+PI^- and live cells as ANV^-PI^- on a FACScan analyzer (Becton, Dickinson and Company, CA, USA). For binding assay, untreated (neither CPT-DMSO nor DMSO mixed), vehicle-treated and CPT-treated Jurkat T-cells were incubated with approximately 66.6 MBq ^{123}I-ANV, ^{123}I-ANV-6L15, or ^{123}I-NH_4I, respectively, in 0.5 mL binding buffer (10 mM HEPES, 137 mM NaCl, 4 mM KCl, 0.5 mM $MgCl_2$, 0.5 mM NaH_2PO_4, 0.1% glucose, 0.1% BSA, 1.2 mM $CaCl_2$, pH 7.4) at room temperature for 15 min. The cells were pelleted, washed once with the binding buffer, and resuspended in the same buffer. The radioactivity bound to the cells was measured using an automatic gamma counter (Wallac 1470 Wizard).

2.6. Biodistribution and Imaging of Radioiodinated ANV-6L15. All animal experiments were approved by the Institutional Animal Care and Use Committee (IACUC) of INER. All animals were kept in a temperature-controlled room (at 22.5 ± 2°C) with illumination cycle of 12 hours per day and were maintained on a standard diet (Lab diet; PMI Feeds, St. Louis, MO, USA) with free access to tap water.

For biodistribution study, 18 eight-week-old male BALB/c mice (obtained from the National Animal Center, Taipei, Taiwan) were injected intravenously via the lateral tail vein with 444 ± 37 kBq ^{123}I-ANV-6L15 and sacrificed at 2, 10, 30, 60, 120, and 180 min after injection (three mice for each time point) under isoflurane anesthesia. Blockade of specific uptake of free iodide was achieved by intraperitoneal injection of KI (3.9 mg per mouse) 30 min before radiotracer injection. At the selected time, main organs and tissues were obtained, weighed, and counted for radioactivity on a Wallac 1470 gamma counter. The distribution data were expressed as percentage of the injected dose per organ (%ID/organ) and per gram of tissue (%ID/g).

For *in vivo* imaging study, one BALB/c mouse was injected via tail vein with 18.5 MBq of ^{123}I-ANV-6L15 in physiological saline (100 μL). Under isoflurane anesthesia, whole body scans were acquired on an X-SPECT (Gamma Medica, Northridge, CA, USA) equipped with an HRES (high resolution electronic system) collimator 60–210 min after injection.

Table 1: Labeling yields and radiochemical purities of radioiodinated ANV and radioiodinated ANV-6L15.

	Labeling yield (%)	Radiochemical purity (%)	
^{123}I-ANV	51.4 ± 8.4	96.0 ± 3.9	(n = 7)
^{123}I-ANV-6L15	44.2 ± 4.9	98.0 ± 2.6	(n = 6)
^{125}I-ANV	74.0 ± 6.6	97.6 ± 1.0	(n = 4)
^{125}I-ANV-6L15	74.5 ± 7.3	96.1 ± 1.4	(n = 4)

Data expressed as mean ± SD.

2.7. Statistical Analysis. Data were expressed as mean ± standard deviation (SD). The binding of ^{123}I-ANV and ^{123}I-ANV-6L15 in CPT-treated Jurkat T-cells were compared using Student's t-test, with $P < .05$ indicating statistical significance.

3. Results and Discussion

3.1. Radiochemical Profile of Radioiodinated Proteins. ANV-6L15 as well as native ANV were successfully labeled with radioiodine using Iodogen method. The representative size-exclusion chromatograms of radioiodinated ANV and ANV-6L15 were shown in Figure 1. The retention times of radioiodinated ANV, ANV-6L15, and radioiodide were 8.33 ± 0.07 min, 9.20 ± 0.15 min, and 15.5 ± 0.25 min, respectively. Since the molecular weight of ANV-6L15 (contains 378 amino acids) is larger than that of ANV (contains 319 amino acids), the slightly longer retention time of radioiodinated ANV-6L15 compared to that of ^{123}I-ANV possibly reflected the difference in molecular conformation and/or interaction with the chromatographic medium rather than the difference in molecular size. The labeling yields of ^{123}I-ANV, ^{123}I-ANV-6L15, ^{125}I-ANV, and ^{125}I-ANV-6L15 were 51.4 ± 8.4%, 44.2 ± 4.9%, 74.0 ± 6.6%, and 74.5 ± 7.3%, respectively. The radiochemical purities of ^{123}I-ANV, ^{123}I-ANV-6L15, ^{125}I-ANV, and ^{125}I-ANV-6L15 were 96.0 ± 3.9%, 98.0 ± 2.6%, 97.6 ± 1.0%, and 96.1 ± 1.4%, respectively (Table 1).

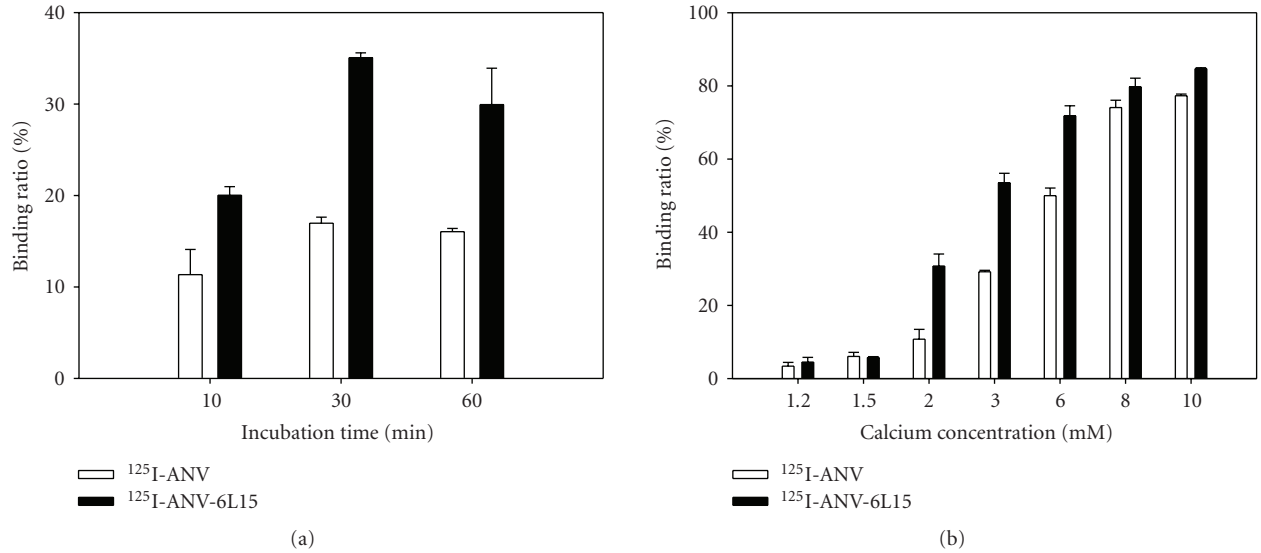

Figure 2: Binding of ^{125}I-ANV and ^{125}I-ANV-6L15 to erythrocyte ghosts. (a) Time course of binding of ^{125}I-ANV or ^{125}I-ANV-6L15 to ghost erythrocytes in the presence of 2.5 mM Ca^{2+} at room temperature. (b) Binding of ^{125}I-ANV or ^{125}I-ANV-6L15 to ghost erythrocytes under various concentrations of Ca^{2+}. Data are expressed as mean ± SD of three independent experiments.

The radioiodinated proteins were stable at room temperature for up to 10 hours (data not shown).

The most commonly used techniques for radioiodination of proteins are Iodogen, Iodobead and chloramine-T methods. Previously reported labeling yields of radioiodinated ANV using Iodogen and Iodobead were 70% and 40%, respectively [13, 14, 17]. The labeling yields of radioiodinated ANV and ANV-6L15 in this study were comparable with the data reported in the literature.

Due to limited availability of ^{123}I, we used ^{123}I mainly for animal studies (biodistribution and SPECT imaging) and related Jurkat T-cell binding assay. To prevent frequent shortage of ^{123}I during the course of study, we used relatively longer half-lived and commercially available ^{125}I for in vitro study on erythrocyte ghost cell. We assume similar binding characteristics between radiolabels of ^{123}I and ^{125}I.

3.2. Erythrocyte Ghost Binding Assay. To determine whether ANV-6L15 maintained its biological activity after radioiodination, erythrocyte ghost binding assay was performed. The results showed that the binding of ^{125}I-ANV or ^{125}I-ANV-6L15 to erythrocyte ghosts was time- and Ca^{2+}-dependent (Figures 2(a) and 2(b)). Maximal binding of either ^{125}I-ANV or ^{125}I-ANV-6L15 to erythrocyte ghosts occurred after 30 min incubation in the presence of 2.5 mM Ca^{2+}; the binding ratio was 16.97 ± 0.66% and 35.07 ± 0.53% for ^{125}I-ANV and ^{125}I-ANV-6L15, respectively (Figure 2(a)). The binding of either radioiodinated protein to erythrocyte ghosts steeply increased as Ca^{2+} concentration increased from 1.2 mM to 10 mM, and the binding ratio reached 77.3 ± 0.45% and 84.7 ± 0.26% for ^{125}I-ANV and ^{125}I-ANV-6L15, respectively, at 10 mM Ca^{2+} (Figure 2(b)). ^{125}I-ANV-6L15 exhibited higher binding ratios than ^{125}I-ANV (Figures 2(a) and 2(b)). Thus, radioiodinated ANV-6L15 appeared to possess a higher affinity to membrane PS-binding sites compared to radioiodinated ANV.

Lahorte et al. [13] reported that the optimal incubation time for maximal platelet binding was 20 min or longer in the presence of 5 mM Ca^{2+} and reached a plateau at 20 mM Ca^{2+} when incubated for 30 min. Our data showed that the maximal binding of either ^{125}I-ANV or ^{125}I-ANV-6L15 to erythrocyte ghosts appeared at 30 min in the presence of 2.5 mM Ca^{2+} and reached a plateau at 8 mM Ca^{2+} when incubated for 30 min.

The mechanism for the increased binding affinity of ANV-6L15 for erythrocyte membranes compared with ANV is currently unknown. The coexpression of phosphatidylethanolamine (PE) on the erythrocyte membranes was proposed to contribute importantly to the increased affinity of ANV-6L15 compared with ANV [12].

3.3. Apoptotic Cell Binding Assays. Figure 3 showed a typical flow cytometric dot plot for the untreated and apoptotic CPT-treated Jurkat T-cells. An increased proportion of apoptotic (ANV^+PI^-) and necrotic (ANV^+PI^+) cells was observed in CPT-treated cells. The binding of ^{123}I-ANV-6L15 to CPT-treated cells (23.3 ± 2.1 cpm/10^4 cells) was significantly higher than those of untreated- (8.2 ± 0.4 cpm/10^4 cells) and vehicle- (DMSO-) treated Jurkat T-cells ($P < .03$; Figure 4). In contrast, the binding of ^{123}I-ANV (approximately 4 cpm/10^4 cells) or ^{123}I-iodide (<1 cpm/10^4 cells) was far below those of ^{123}I-ANV-6L15 among different groups, and no increase of ^{123}I-ANV binding to apoptotic Jurkat T-cells was observed (Figure 4). The lack of increased ^{123}I-ANV binding to apoptotic Jurkat T-cells was possibly due to relatively low binding affinity of ^{123}I-ANV for PS-exposed membranes at the physiological concentration Ca^{2+} (1.2 mM).

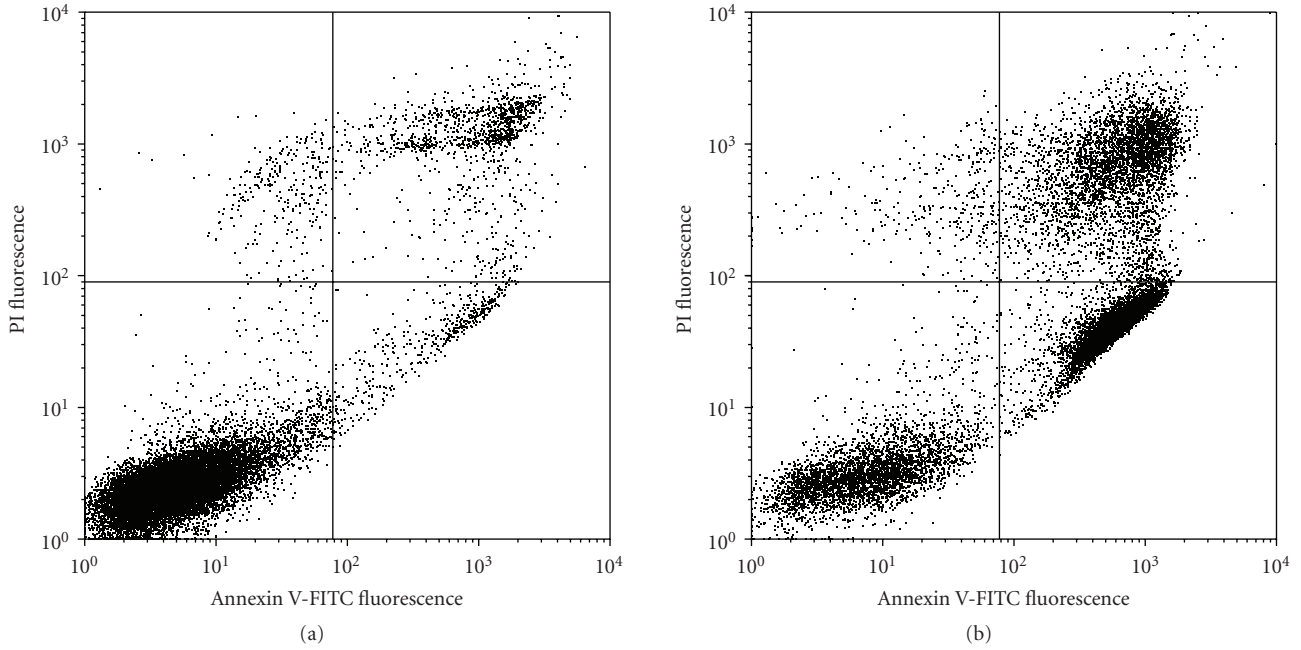

Figure 3: Representative flow cytometric histograms of apoptotic Jurkat T-cells stained with annexin V-FITC and propidium iodide (PI). Jurkat T-cells (2×10^6/mL) were left untreated or treated with camptothecin (CPT, 8 μM) at 37°C for 24 h, followed by staining with ANV-FITC and PI. Apoptotic cells were identified as ANV^+PI^- and live cells as ANV^-PI^- on an FACScan analyser.

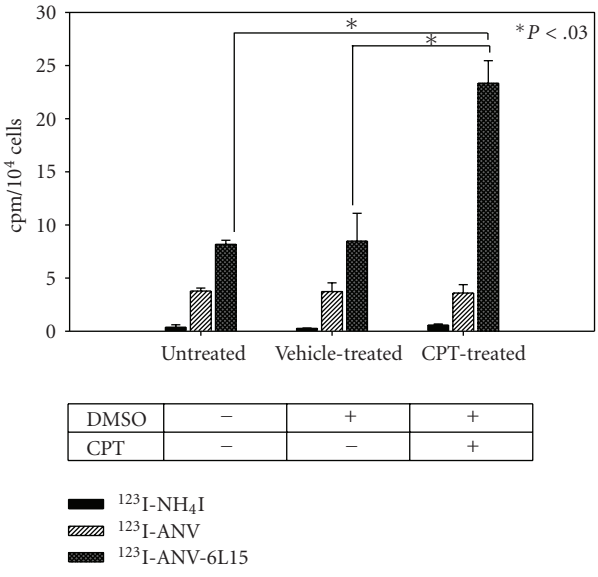

Figure 4: Binding of ^{123}I-ANV and ^{123}I-ANV-6L15 to apoptotic Jurkat T-cells. Jurkat T-cells were either left untreated or treated with camptothecin (CPT, 8 μM) and/or vehicle (5 μL DMSO).

3.4. Biodistribution and Imaging of Radioiodinated ANV-6L15 in Mice. The biodistribution of ^{123}I-ANV-6L15 in BALB/c mice are depicted in Table 2. After bolus injection via tail vein (approximately 25 ng protein/mouse), ^{123}I-ANV-6L15 showed an initial rapid clearance from the blood (40.01 ± 6.25% and 12.29 ± 1.22% ID/organ at 2 min and 60 min after injection, resp.). The liver had the highest radioactivity (11.40 ± 1.34% ID/organ) at 2 min after injection. The organ with the second highest radioactivity was the kidneys (8.61 ± 0.35% ID/organ at 10 min after injection). ^{123}I-ANV-6L15 fusion protein did not cross the blood-brain barrier as indicated by the low brain uptake (<0.5% ID/g in average). Low uptake in the thyroid reflected low level of radioiodide dissociation from the radiolabeled protein *in vivo*. The slight increase of thyroid uptake at 120 and 180 min could be due to *in vivo* ^{123}I dissociation from the radiolabeled protein.

As reported previously [3, 14], ^{123}I-ANV was rapidly cleared from the blood following a biexponential decay and predominant uptake in the kidneys, liver, and gastrointestinal tract. The result of this study revealed that ^{123}I-ANV-6L15 also excreted via kidneys.

In vivo imaging of ^{123}I-ANV-6L15 distribution in a BALB/c mouse after bolus injection via tail vein (approximately 1 μg protein/mouse) showed high uptake of the tracer in the liver and the kidneys (Figure 5). The uptake of ^{123}I-ANV-6L15 in these organs may limit the evaluation of apoptosis in abdominal regions. Further studies of biodistribution and SPECT imaging will be performed at later time points. We will conduct dosimetry calculation for ^{123}I-ANV-6L15 and compare with ^{123}I-ANV. The novel tracer will be evaluated in animal models with stress-induced apoptosis in the future.

Table 2: Biodistribution of ^{123}I-ANV-6L15 fusion protein in healthy BALB/c mice ($n = 3$).

Organ	%ID/organ						%ID/g of tissue					
	2 min	10 min	30 min	60 min	120 min	180 min	2 min	10 min	30 min	60 min	120 min	180 min
Brain	0.29 ± 0.07	0.22 ± 0.07	0.15 ± 0.02	0.13 ± 0.03	0.11 ± 0.03	0.13 ± 0.06	0.74 ± 0.16	0.54 ± 0.26	0.38 ± 0.05	0.32 ± 0.06	0.28 ± 0.03	0.33 ± 0.18
Thyroid	0.39 ± 0.05	0.25 ± 0.06	0.37 ± 0.03	0.34 ± 0.06	0.59 ± 0.09	0.49 ± 0.03	2.47 ± 0.20	1.93 ± 0.61	2.14 ± 0.03	2.15 ± 0.15	3.37 ± 1.17	3.01 ± 0.12
Heart	1.02 ± 0.45	0.58 ± 0.01	0.45 ± 0.14	0.32 ± 0.09	0.33 ± 0.09	0.21 ± 0.04	7.50 ± 2.48	4.36 ± 0.21	3.44 ± 0.56	2.41 ± 0.67	2.45 ± 0.51	1.70 ± 0.42
Lung	2.12 ± 0.32	1.54 ± 0.05	1.00 ± 0.30	0.85 ± 0.28	0.89 ± 0.24	0.54 ± 0.18	14.8 ± 1.19	11.1 ± 2.09	8.65 ± 1.53	5.51 ± 1.31	6.08 ± 0.32	4.49 ± 0.20
Liver	11.40 ± 1.34	11.16 ± 0.73	6.53 ± 0.52	3.33 ± 1.23	3.30 ± 0.26	2.66 ± 0.51	9.20 ± 1.04	8.56 ± 2.49	5.10 ± 0.54	3.01 ± 0.32	2.78 ± 0.46	2.09 ± 0.32
Spleen	0.66 ± 0.19	1.06 ± 0.12	0.88 ± 0.07	0.58 ± 0.09	0.51 ± 0.08	0.35 ± 0.06	7.53 ± 1.66	9.65 ± 1.06	9.61 ± 1.6	5.99 ± 0.33	5.15 ± 0.86	3.75 ± 0.53
Stomach	0.16 ± 0.08	0.25 ± 0.39	0.39 ± 0.09	0.49 ± 0.01	0.70 ± 0.52	0.79 ± 0.38	1.29 ± 0.46	1.42 ± 0.09	3.13 ± 0.24	3.08 ± 0.21	4.56 ± 3.35	5.11 ± 2.21
Intestine	0.05 ± 0.03	0.07 ± 0.00	0.09 ± 0.03	0.11 ± 0.02	0.12 ± 0.03	0.09 ± 0.05	1.08 ± 0.13	1.36 ± 0.18	2.06 ± 0.23	2.20 ± 0.56	1.95 ± 0.56	1.74 ± 0.85
Kidneys	5.23 ± 0.74	8.61 ± 0.35	5.72 ± 1.12	2.95 ± 0.46	2.33 ± 0.02	1.88 ± 0.32	13.57 ± 2.76	21.11 ± 3.31	14.97 ± 3.48	8.22 ± 1.99	5.75 ± 0.61	4.63 ± 0.74
Bladder	0.06 ± 0.03	0.05 ± 0.01	0.15 ± 0.10	0.14 ± 0.08	0.07 ± 0.02	0.13 ± 0.09	1.42 ± 1.16	2.13 ± 0.76	4.76 ± 2.62	5.40 ± 2.70	2.37 ± 0.49	6.24 ± 6.14
Urine	0.01 ± 0.01	0.14 ± 0.2	1.02 ± 1.12	2.36 ± 1.57	0.13 ± 0.22	1.64 ± 2.72	12.13 ± 15.9	11.41 ± 16.13	32.75 ± 2.19	80.92 ± 51.1	18.58 ± 22.31	50.03 ± 7.25
Testis	0.11 ± 0.02	0.10 ± 0.01	0.16 ± 0.02	0.16 ± 0.02	0.25 ± 0.02	0.25 ± 0.05	0.71 ± 0.16	0.62 ± 0.08	1.05 ± 0.08	1.04 ± 0.09	1.72 ± 0.33	1.50 ± 0.33
Blood*	40.01 ± 6.25	25.07 ± 0.35	16.30 ± 1.8	12.29 ± 0.22	11.96 ± 0.13	9.19 ± 0.82	26.21 ± 3.17	15.91 ± 2.35	10.46 ± 0.67	7.91 ± 1.01	7.55 ± 1.05	5.79 ± 0.51
Muscle#	6.68 ± 0.74	5.91 ± 0.29	7.31 ± 1.79	7.88 ± 2.62	8.84 ± 1.12	6.52 ± 2.78	0.77 ± 0.08	0.66 ± 0.09	0.82 ± 0.16	0.90 ± 0.32	0.97 ± 0.11	0.72 ± 0.31
Bone+	3.68 ± 0.80	3.09 ± 0.38	2.61 ± 0.65	2.33 ± 0.88	3.55 ± 0.34	2.73 ± 0.15	2.60 ± 0.54	2.12 ± 0.46	1.80 ± 0.35	1.62 ± 0.63	2.42 ± 0.34	1.85 ± 0.12

*Estimated total blood volume: 7.0% of total body weight.
#Estimated total muscle: 40.0% of total body weight.
+Estimated total bone: 6.5% of total body weight.
%ID: percentage of injected dose.
Data expressed as mean ± SD.

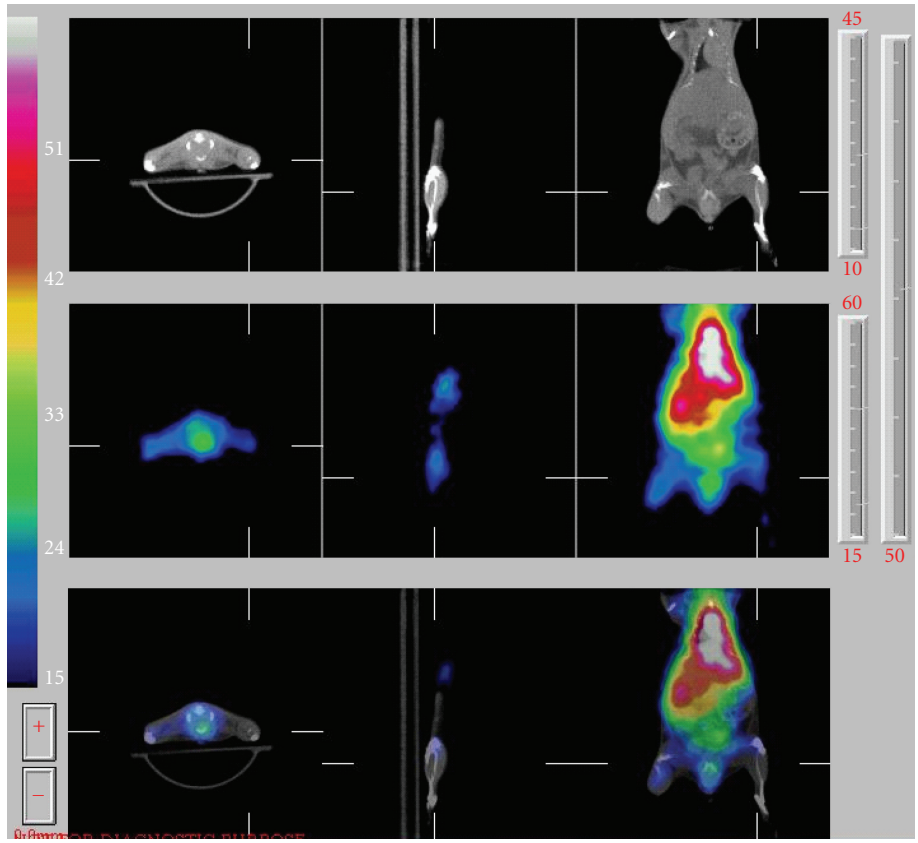

Figure 5: *In vivo* SPECT images of ^{123}I-ANV-6L15 fusion protein in an eight-week-old male BALB/c mouse. ^{123}I-ANV-6L15 (18.5 MBq in 100 μL physiological saline) was injected via tail vein of the mouse under isoflurane anesthesia. Whole body scan was acquired at 60–210 min after injection.

4. Conclusions

ANV-6L15 was successfully labeled with radioiodine using Iodogen method. Radioiodinated ANV-6L15 showed significantly higher binding to PS-exposed erythrocyte ghosts and camptothecin-induced apoptotic Jurkat T-cells at physiological concentration of Ca^{2+} compared to that of radioiodinated ANV *in vitro*. Biodistribution study showed that ^{123}I-ANV-6L15 was rapidly cleared from the blood. Further imaging studies in animal models of apoptosis are warranted. Owing to higher binding affinity to PS, radioiodinated ANV-6L15 could be more sensitive than radioiodinated ANV to detect the apoptosis-associated treatment and human disorders, such as radiation/chemotherapy efficacy, myocardial ischemia or infarct, infectious diseases, and neurodegenerative diseases. Taken together, these results suggest that the radioiodinated ANV-6L15 may be a better scintigraphic tracer for apoptosis detection compared with ANV.

Acknowledgments

The authors are indebted to Dr. Wuu-Jyh Lin for providing ^{123}I-NH_4I. The technical support of binding assay from Dr. Mei-Ping Kung is acknowledged. This paper was supported partially by Grants from the National Science Council, Taiwan (NSC 96-2001-01-06-00-00 and INER 972001INER056 to S.-P. Wey) and National Heart, Lung, and Blood Institute, USA (1R43HL093848-01A1 to T.-C. Wun).

References

[1] F. G. Blankenberg, P. D. Katsikis, J. F. Tait et al., "Imaging of apoptosis (programmed cell death) with ^{99m}Tc annexin V," *Journal of Nuclear Medicine*, vol. 40, no. 1, pp. 184–191, 1999.

[2] J. F. Taiy, "Imaging of apoptosis," *Journal of Nuclear Medicine*, vol. 49, pp. 1573–1576, 2008.

[3] C. M. M. Lahorte, J. L. Vanderheyden, N. Steinmetz, C. V. De Wiele, R. A. Dierckx, and G. Slegers, "Apoptosis-detecting radioligands: current state of the art and future perspectives," *European Journal of Nuclear Medicine and Molecular Imaging*, vol. 31, no. 6, pp. 887–919, 2004.

[4] M. Subbarayan, U. O. Häfeli, D. K. Feyes, J. Unnithan, S. N. Emancipator, and H. Mukhtar, "A simplified method for preparation of ^{99m}Tc-annexin V and its biologic evaluation for in vivo imaging of apoptosis after photodynamic therapy," *Journal of Nuclear Medicine*, vol. 44, no. 4, pp. 650–656, 2003.

[5] R. F. A. Zwaal and A. J. Schroit, "Pathophysiologic implications of membrane phospholipid asymmetry in blood cells," *Blood*, vol. 89, no. 4, pp. 1121–1132, 1997.

[6] E. Kazuo, T. S. Noriko, K. Hajime, I. Keizo, and U. Masato, "Exposure of phosphatidylethanolamine on the surface of apoptotic cells," *Experimental Cell Research*, vol. 232, no. 2, pp. 430–434, 1997.

[7] B. L. Wood, D. F. Gibson, and J. F. Tait, "Increased erythrocyte phosphatidylserine exposure in sickle cell disease: flow-cytometric measurement and clinical associations," *Blood*, vol. 88, no. 5, pp. 1873–1880, 1996.

[8] J. F. Tait, C. Smith, Z. Levashova, B. Patel, F. G. Blankenberg, and J. L. Vanderheyden, "Improved detection of cell death in vivo with annexin V radiolabeled by site-specific methods," *Journal of Nuclear Medicine*, vol. 47, no. 9, pp. 1546–1583, 2006.

[9] G. Niu and X. Chen, "Apoptosis imaging: beyond annexin V," *Journal of Nuclear Medicine*, vol. 51, pp. 1659–1662, 2010.

[10] W. L. Van Heerde, P. G. De Groot, and C. P. M. Reutelingsperger, "The complexity of the phospholipid binding protein annexin V," *Thrombosis and Haemostasis*, vol. 73, no. 2, pp. 172–179, 1995.

[11] H. H. Chen, C. P. Vicente, LI. He, D. M. Tollefsen, and T. C. Wun, "Fusion proteins comprising annexin V and Kunitz protease inhibitors are highly potent thrombogenic site-directed anticoagulants," *Blood*, vol. 105, no. 10, pp. 3902–3909, 2005.

[12] T.-C. Yen, S.-P. Wey, C.-H. Liao et al., "Measurement of the binding parameters of annexin derivative-erythrocyte membrane interactions," *Analytical Biochemistry*, vol. 406, no. 1, pp. 70–79, 2010.

[13] C. Lahorte, G. Slegers, J. Philippé, C. Van de Wiele, and R. A. Dierckx, "Synthesis and in vitro evaluation of ^{123}I-labelled human recombinant annexin V," *Biomolecular Engineering*, vol. 17, no. 2, pp. 51–53, 2001.

[14] C. M. Lahorte, C. van de Wiele, K. Bacher et al., "Biodistribution and dosimetry study of ^{123}I-rh-annexin V in mice and humans," *Nuclear Medicine Communications*, vol. 24, no. 8, pp. 871–880, 2003.

[15] B. Dekker, H. Keen, S. Lyons et al., "MBP-annexin V radiolabeled directly with iodine-124 can be used to image apoptosis in vivo using PET," *Nuclear Medicine and Biology*, vol. 32, no. 3, pp. 241–252, 2005.

[16] H. G. Keen, B. A. Dekker, L. Disley et al., "Imaging apoptosis in vivo using ^{124}I-annexin V and PET," *Nuclear Medicine and Biology*, vol. 32, no. 4, pp. 395–402, 2005.

[17] J. Russell, J. A. O'Donoghue, R. Finn et al., "Iodination of annexin V for imaging apoptosis," *Journal of Nuclear Medicine*, vol. 43, no. 5, pp. 671–677, 2002.